2014 5th IEEE RAS & EMBS International Conference on
Biomedical Robotics and Biomechatronics (BioRob)
August 12-15, 2014. São Paulo, Brazil

Achilles: An Autonomous Lightweight Ankle Exoskeleton to Provide Push-Off Power

Cor Meijneke*, Wietse van Dijk*, and Herman van der Kooij, *Member, IEEE*

Abstract— **This paper presents the Achilles exoskeleton, an autonomous ankle exoskeleton that can generate 52% of the positive plantarflexion power around the ankle of a 80 kg individual with only 1.5 kg of mass added around the ankle joint. The mass of the exoskeleton is lower and the power density is higher than that of existing autonomous exoskeletons. This high power density was achieved by designing a series elastic actuator that consists of an electric motor and ball-screw gear with a carbon fiber reinforced leaf-spring as lever-arm. A dynamic model that includes the motor and gear properties, spring stiffness, and exoskeleton geometry was used to optimize the design parameters for positive power injection. Doing this for multiple combinations of preselected motors and gears and comparing their support to weight ratio, revealed the best drive combination. The performance of the realized exoskeleton was assessed in several tests. The actuator can track the optimized actuator stroke trajectory with a following error that has a RMS of 2.3 mm, it can track force reference signals with amplitudes of 1 N to 100 N with a bandwidth between 8.1 Hz and 20.6 Hz, and it outputs a maximum mechanical power of 80.2 W. These results show that the device is suitable for fulfilling its purpose: reducing the metabolic cost of walking with an autonomous device.**

I. Introduction

It is hypothesized that humans can improve their mobility by wearing an exoskeleton. A key improvement is the reduction of the metabolic cost of walking [1]. The metabolic cost of walking is for a large part determined by the positive power provided in the trailing leg that compensates the impact losses that occur in the front leg around heel strike [2]. The positive power is for a large part provided by the ankle joint, making it a suitable candidate for exoskeletal support [3], [4].

Recent experimental research has shown that the metabolic cost of walking can indeed be reduced with an ankle exoskeleton that supports the push-off of the trailing leg [5].The downside of this, and other [4], [6] exoskeletons, is that they rely on pneumatic muscles with an external power source. This prohibits the autonomous operation of the exoskeletons that is required for real-life applications. Alternatively, different autonomous exoskeletons have been developed that rely on electric actuators (e.g. [7], [8]). Unfortunately these exoskeletons have been less successful in reducing metabolic cost than their pneumatic equivalents.

The power density, the ratio between the power and the mass, of electric motors and gearboxes is much lower than for pneumatic muscles, which are nothing more than a fiber reinforced inflatable tube. The mass of the electric actuator, and the placement of the actuator at the ankle has a large effect on the metabolic cost [9], [10]. This is problematic because high power is required to give a significant amount of support.

Another advantage of the pneumatic muscles is that they have an intrinsic compliance. A compliant electric actuator can be made by placing a spring in series with the motor (series elastic actuation, SEA). SEA has been applied in various exoskeletons [11]–[13].

Using SEA at the ankle has an additional advantage. During the stance phase, the ankle joint provides both negative and positive power. The negative power can be used for temporal energy storage in the spring, leading to lower power requirements on the actuator. This is analogue to the elastic recoil of the Achilles tendon reducing the power provided by the plantarflexors [14], [15]. Using SEA an electric exoskeleton was build. However the power density of this exoskeleton was still much lower than existing pneumatic exoskeletons [5], [12].

For successful autonomous exoskeletons the power density has to be further increased. This requires a minimalistic lightweight design. The mass of the SEA can be kept at a minimum by using an integral optimization that determines choice of the motor, transmission, and spring characteristics [16]. The components that interface between the SEA and the human should be minimal in number and mass. This can be achieved by using function integration.

Goal of this paper is to design an autonomous ankle exoskeleton that reduces the metabolic cost of walking. We will show that our exoskeleton outperforms existing autonomous exoskeletons with its lightweight design and high power density. The paper describes the working principle, optimization of the motor, gear and spring characteristics, and performance assessment of the exoskeleton.

II. Methods

A. Design

1) Working principle

The exoskeleton is build up from a linear actuator, that consists of a rotary electric motor and ball-screw gear, which

* Authors have equal contributions to this article

C. Meijneke, W. van Dijk, and H. van der Kooij are with the Biomechanical Engineering Laboratory, Faculty of Mechanical, Maritime and Materials Engineering, Delft University of Technology, Mekelweg 2, 2628 CD Delft, The Netherlands. H. van der Kooij is also with the Biomechanical Engineering Laboratory, Institute for Biomedical Technology and Technical Medicine (MIRA), University of Twente, Drienerlolaan 5, 7500 AE Enschede, The Netherlands. (contacts are respectively: c.meijneke@tudelft.nl +31-152783986, w.vandijk@tudelft.nl and h.vanderkooij@ctw.utwente.nl)

The work presented here was supported by the EU within the SYMBITRON project (FP7-ICT-2013-10 contract #611626).

is suspended in a linkage mechanism between the shank and foot shells. The link, or lever-arm, that is attached to the foot shell is flexible thus introduces the series elasticity (Figure 1).

2) Mechanical model

The support torque (T_s) is given by the equivalent linear rotational spring stiffness (c_s) and the spring deformation angle (q_s):

$$T_s(c_s, q_j(t), x_m(t), r_1, r_2, \psi) = c_s \cdot q_s(q_j(t), x_m(t), r_1, r_2, \psi) \quad (1)$$

The spring deformation is a function of the joint angle ($q_j(t)$), the motor stroke trajectory ($x_m(t)$) that are both changing over time (t), and the exoskeleton dimensions (*r1*, *r2* and ψ), and can be calculated using trigonometric functions (Figure 1).

The dynamics of the system are given in Figure 1. Throughout the document we assume that we know the joint angle ($q_j(t)$) and the total joint torque ($T_j(t)$) and use data from [17] (data from normal walking) as a reference. This leaves the design parameters r_1, r_2 and ψ, and the motor stoke trajectory $x_m(t)$. The dynamic equilibrium equations can be written as:

$$M_{eq}\ddot{x}_m(t) = \Sigma F(t) = F_m(t) + F_s(t) \quad (2)$$

where M_{eq} is the equivalent mass combining the reflected mass of the motor and gear inertia. F_m is equivalent motor force. The force in the spindle F_s depends on the angle between the actuator axis and lever-arm $\gamma(x_m(t), r_1, r_2)$ and is given by:

$$F_s(t) = \frac{T_s(t)}{r_2 \sin(\gamma(t))} \quad (3)$$

The motor stroke and force $x_m(t)$ and $F_m(t)$ are linearly related with the motor angle ($q_m(t)$) and torque ($T_m(t)$) by the transmission ratio of the ball-screw:

$$R_s = \frac{p_s}{2\pi} \quad (4)$$

where p_s is the pitch of the ball-screw.

3) Optimization

The main goal in the actuation system design was to supply the highest amount of support to with the smallest added mass to the ankle. This was achieved by using an optimization process similar to [16]. The dimensions of the linkage mechanism and stiffness of the flexible lever-arm were optimized for all combinations of preselected motors and gears.

The exoskeleton should provide solely positive power during the push of. The amount of support is therefore captured in the following function:

$$f(z) = 1 - \frac{\int_0^T \left| \max\left(P_j(t), 0\right) - P_s(t, z) \right| dt}{\int_0^T \left| \max\left(P_j(t), 0\right) \right| dt} \quad (5)$$

$P_j(t)$ and $P_s(t)$ are respectively the total joint power and the exoskeleton joint power and $\boldsymbol{z}$ the parameters to be optimized. The support optimization can be formulated as the following maximization problem:

$$\text{maximize } f(\boldsymbol{z}) \text{ subject to } \boldsymbol{g}(\boldsymbol{z}) \le 0 \text{ and } \boldsymbol{lb} \le \boldsymbol{z} \le \boldsymbol{ub} \quad (6)$$

$\boldsymbol{g}(\boldsymbol{z})$ are the electrical and mechanical constraints on the motor and gear. ***lb*** and ***ub*** are the respective lower and upper bounds on the parameters. The optimization parameters are given by:

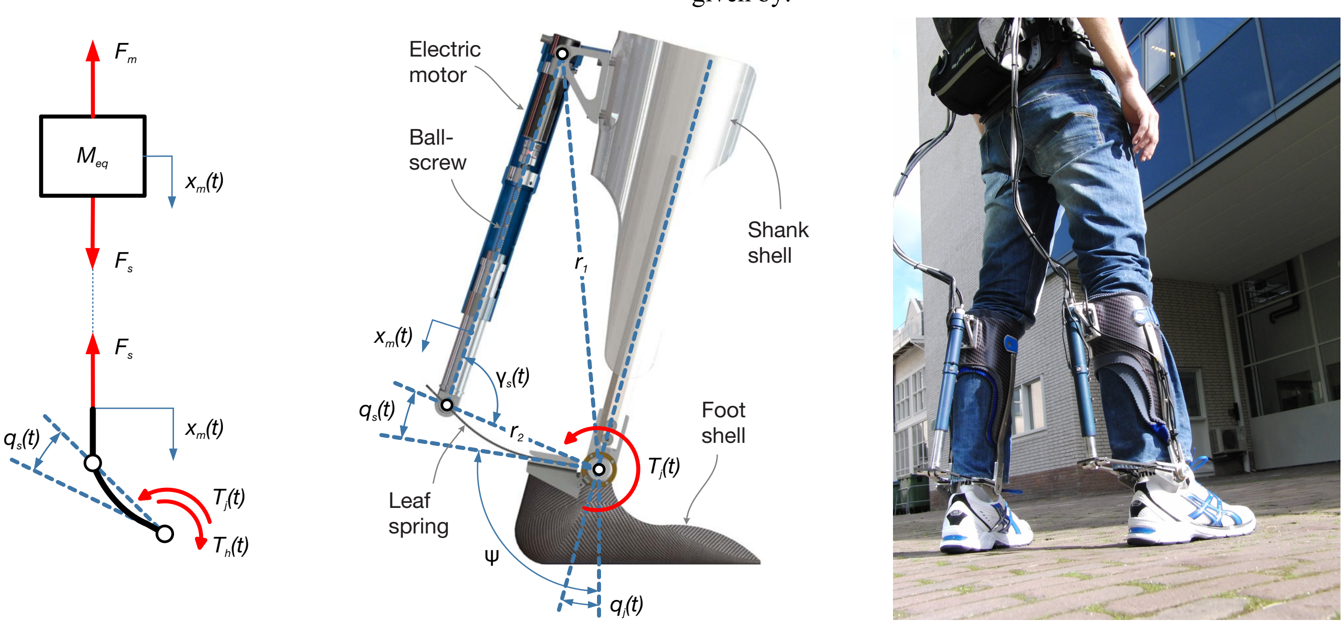

Figure 1: A schematic of the system dynamics (left), the CAD model with a partial cross-section of the actuator (middle), and a photo of the author wearing the Achilles exoskeleton (right). The variables are $x_m(t)$ is the stroke of the actuator, $q_s(t)$ the deflection of the lever-arm, $q_j(t)$ the joint angle, $\gamma(t)$ the angle between the actuator axis and lever-arm, $T_j(t)$ the joint torque, T_h the torque exerted by the human, F_s the spindle force, and F_m the force from the motor. The parameters are r_1 the proximal lever-arm length, r_2 the distal lever-arm length, ψ the distal lever-arm angle, and M_{eq} equivalent mass of the drive components. Note that the schematic of the system dynamics gives no clear distinction between rotational and translational components.

$$z = \{x_m, r_1, r_2, \psi, c_s\} \quad (7)$$

where x_m are the stroke trajectory parameters. These parameters represent 16 points equally distributed over the gait cycle. The stroke function of the actuator $x_m(t)$ is given by smoothed interpolation between these points. The minimization problem is solved by the *fmincon* numerical solver in Matlab (Mathworks, Natick, MA, US). For comparison, the total mass each motor/gear combination was plotted against the amount of power it supplies to the user.

a) Electrical and mechanical constraints

The exoskeleton is subject to mechanical and electrical constraints (Table 1). The motor current (I_m), voltage (U_m) and electrical power (P_m) are calculated using the methods of [16]. The constraint function *g(z)* combines the constraint equations of Table 1 and outputs a vector of which all elements are equal or smaller than zero if and only if all constraints are satisfied.

b) Motor gear combinations

The motors and ball-screw gears that were selected for the optimization are respectively listed in Table 2 and Table 3 along with their relevant specifications. The total mass of each motor/gear combination was calculated by:

$$m_{tot} = m_m + m_{g1} + \hat{m}_{g2}\left(\max\left(x_m(t)\right) - \min\left(x_m(t)\right)\right) \quad (8)$$

4) Spring design

The lever-arm is required to store large amounts of energy. Therefore unidirectional carbon fibre was chosen because of its superior energy density. The spring was cut from a carbon plate with a uniform thickness, hence the design parameters are the thickness and width profile. The correct dimensions were determined using a finite element model of the spring in ANSYS (ANSYS Inc., Cecil Township, PA, US).

5) Control and electronics

The exoskeleton is controlled with a cascaded control scheme. The outer loop of the control regulates the actuator stroke and thereby the spring deflection and force. The inner loop regulates the motor velocity. The loops are respectively PI- and P-controlled [18].

The exoskeleton was controlled using distributed control via the EtherCAT protocol. A NUC computer with Core i3 processor (Intel, Santa Clara, CA, US) running Linux was used as the EtherCAT master. Matlab/Simulink (MathWorks, Natick, MA, US) was used to program the high level control. SOEM (Berlios, Berlin, Germany) and E-box (TU/e, Eindhoven, the Netherlands) were used to implement the EtherCAT master that runs at 1 kHz.

The motors were controlled by EPOS3 70/10 EtherCAT motor controllers (Maxon Motor ag, Sachseln, Switzerland). The joint angle was recorded with an RMB20IC13BC SSI-encoder (RLS-Renishaw, Ljubljana, Slovenia). The motor stroke was recorded by an SCH24-200-D-03-64-3-B incremental encoder (Scancon, Allerød, Danmark) mounted on the motor axis. EK1100 and EL5002 EtherCAT modules (Beckhoff Automation GmbH, Verl, Germany) were used for the incremental encoder interface. The motors and computer are powered by respectively a Zippy Compact 5000mAh 8S 25C and a Zippy Compact 5800 3S 25C Lithium-Polymer battery. The batteries, computer and EhterCAT slaves are mounted in a backpack that can be carried by the user.

TABLE 1: ELECTRICAL AND MECHANICAL CONSTRAINTS

Variable	Description	Constraint equation
$I_m(t)$	Motor current	$\max\left(I_m(t)\right) - I_{\max} < 0$
$U_m(t)$	Motor voltage	$\max\left(U_m(t)\right) - U_{\max} < 0$
$P_m(t)$	Motor power (electrical)	$\max\left(P_m(t)\right) - P_{\max} < 0$
$\dot{q}_m(t)$	Motor speed	$\max\left(\dot{q}_m(t)\right) - \omega_{\max} < 0$
$F_m(t)$	Motor force	$\max\left(F_m(t)\right) - F_{\max} < 0$
$\dot{x}_m(t)$	Spindle velocity	$\max\left(\dot{x}_a(t)\right) - v_{\max} < 0$
$x_a(t)$	Spindle stroke	$\max\left(x_m(t)\right) - \min\left(x_m(t)\right) - L_{\max} < 0$

Overview of the electrical and mechanical constraints on the system. The maximal current was obtained from the guidelines of the manufacturer: $I_{\max} = I_{nom}\sqrt{t_{cycle}/t_{I_m > I_{nom}}}$ where I_{nom} is the nominal current, $t_{I_m > I_{nom}}$ is the ratio between the cycle time and the time the current is above its nominal value per cycle.

TABLE 2: SPECIFICATIONS OF PRESELECTED MOTORS

Property	Symbol	RE35	EC32	EC4p22	EC4p22	Unit
Power rating (electrical)	$P_{\max}$	90	80	90	120	[W]
Winding voltage	$U_{\max}$	24	24	24	24	[V]
Nominal current	I_{nom}	3.47	2.44	3.88	4.81	[A]
Motor mass	m_m	360	270	125	175	[g]
Rotor inertia	J_m	3350	2000	554	891	[g·mm^2]
Max speed	$\omega_{\max}$	12000	25000	25000	25000	[rpm]

Supplier of all listed motor types is Maxon (Maxon Motor ag, Sachseln, Switzerland)

TABLE 3: SPECIFICATIONS OF PRESELECTED BALL-SCREW GEARS

Property	Symbol	SH6x2	SD8x2.5	SD10x2	SD10x4	Unit
Spindle pitch	p_s	2	2.5	2	4	[mm]
Max feed velocity	$v_{\max}$	277	260	166	332	[mm/s]
Max spindle load	$F_{\max}$	1500	2600	3500	5400	[N]
Nut mass	m_{g1}	25	25	30	40	[g]
Spindle specific mass	$\hat{m}_{g2}$	0.180	0.320	0.510	0.430	[g/mm]
Spindle specific inertia	$\hat{J}_g$	0.07	0.21	0.52	0.38	[g·mm]

Supplier of all listed ball-screw gears is SKF (SKF, Gothenburg, Sweden)

B. Assessment

1) Lever-arm stiffness

The stiffness of the produced spring was compared to the estimated stiffness. The stiffness is nonlinear and to obtain the exact stiffness characteristic ($T_s(q_s)$) of the spring, a force-travel experiment was performed. The spring was mounted on a table edge using the same mounting components as in the exoskeleton. A platform was connected to the endpoint of the spring via a cable and incrementally loaded with 1, 3, 8, 13, 18, 23, 25 and 35 kg. The travel (x_s) of the endpoint was measured with a digital caliper with respect to a reference plate that was fixed to the table.

2) Stroke tracking

It was evaluated how well the actuator could track the optimized stroke trajectory. During this test the exoskeleton was mounted such that it could freely move and the optimized stroke trajectory was sent to the controller. The achieved stroke was recorded. The RMS of the tracking error, the difference between the input and output value, was taken as the tracking performance.

3) Force bandwidth

The force bandwidth gives an indication of how well the actuator could follow a force signal. To test the force bandwidth the series elastic actuator was placed between two fixed endpoints Figure 2. A sine sweep signal from 1 Hz to 30 Hz was fed to the controller. The amplitude of the signal ranged from 1 N to 100 N with an offset equal to the amplitude (so the maximal force was twice the amplitude and the actuator only exerted plantarflexion torques, which is the intended use). For each amplitude the crossover frequency (at -3dB) was determined.

4) Power

The mechanical power output of the actuator is evaluated with the same setup as used for the force bandwidth test (Figure 2). The test simulates the loading of the spring during walking. The test starts with no deflection of the spring. From this start point the spring is loaded by sending the maximal allowable input to the actuator. The deflection of the spring is recorded. This gives the force in the spring (see lever arm stiffness) and the speed of the actuator, the product of the two gives the power output of the actuator.

III. Results

A. Design

The actuation system was successfully optimized for all combinations of motors and gearboxes. The resulting support (*f*) and total mass (m_{tot}) of each combination is plotted in Figure 3. From the three combinations on the pareto front, the middle one was chosen for implementation which is a Maxon EC22 4 pole motor with a SH6x2 ball-screw gear. With this drive combination, the actuation system can exert up to 192 W of power around the ankle of an 80 kg person. The full power characteristics are shown in Figure 4. The mass of the motor and gear combination was 218 g.

The optimal components and parameters were implemented in a CAD model which was manufactured. The mass of the Achilles exoskeleton is 1.5 kg per foot and the backpack has a mass of 5.2 kg (Figure 1). A video of the Achilles exoskeleton, and the tests performed with it, is available as online supplementary material.

B. Assessment

1) Lever-arm stiffness

The predicted and measured lever-arm stiffness is shown in Figure 5. A third-order polynomial was fit through the experimentally obtained data points. The maximal deflection difference in the evaluated working range of the spring between the predicted stiffness and the measured data was 0.92 mm at a force of 30 N.

2) Stroke tracking

Figure 6 shows the tracking performance of the actuator. During this test the actuator tracks the optimized stroke trajectory. The RMS of the tracking error was 2.3 mm.

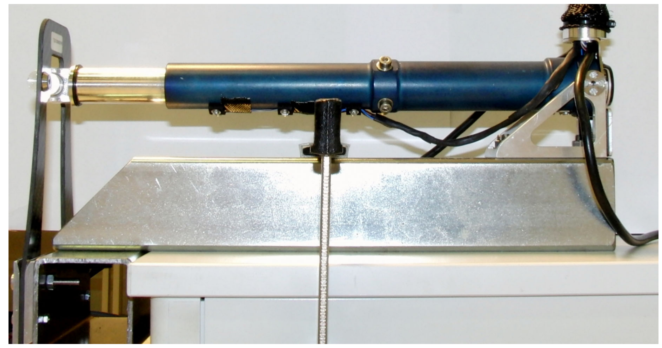

Figure 2: The actuator of the exoskeleton mounted between two rigid endpoints.

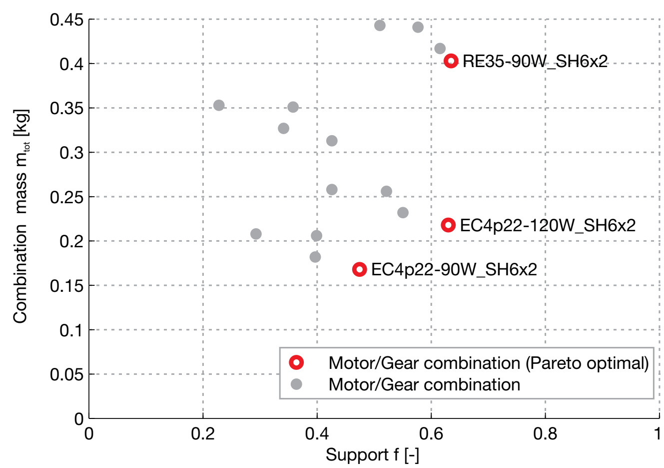

Figure 3: Simulation results of the support given to the user versus total mass of the drive components, where each circle represents an optimization for a motor and gear combination. The three red-thick circles form the Pareto front.

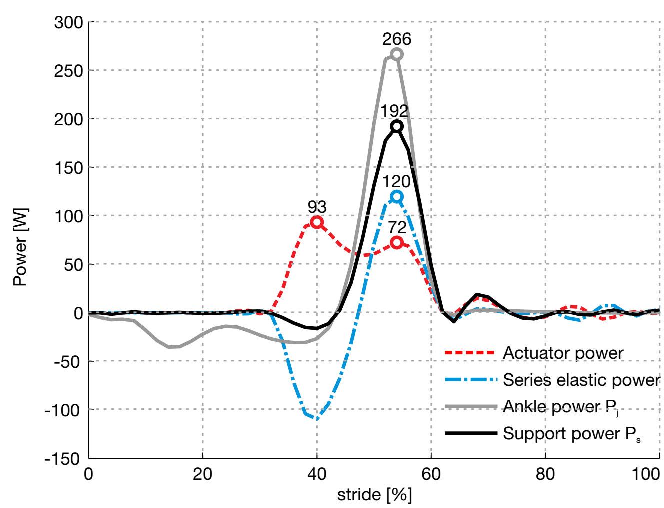

Figure 4: Simulation results of the ankle power as a function of stride with contributions of the motor and spring. The actuator power and the spring power sum up to the support power.

3) Force Bandwidth

The force bandwidth was between 8.1 Hz and 20.6 Hz (Figure 7 and Figure 8). The lowest bandwidth was measured at the highest amplitude (100N).

4) Power

The mechanical power of the actuator is shown in Figure 9. The peak power of the actuator was 80.2W (the model predicted 93.4W peak power) the maximal amount of energy that was stored in the spring is 6.28 J at 34.6 mm deflection.

IV. Discussion

The main contribution of this paper is that we have designed and built an autonomous exoskeleton for plantarflexion support. The optimizations have shown that the Achilles exoskeleton can provide 60.6% of the positive power generated at the ankle during push-off. The power density exceeds that of current autonomous exoskeletons and is similar to that of non-autonomous devices (Table 4).

The high power to weight ratio was achieved by a minimalistic design. The choice for the motor, transmission and spring characteristics was based on optimization results. The spring in the SEA acts as an energy buffer similar to the Achilles tendon. Power losses caused by friction are low due to the use of a ball screw transmission. This largely reduced the required motor power resulting in a weight of the motor and transmission of only 218 g. The elastic element of the SEA and the lever arm function were combined in one leaf spring. This made it possible to make a minimalistic and lightweight design for the interface. Batteries and control electronics are carried on the back where the weight of these components have a much smaller effect on the metabolic cost of walking than if they were placed at the foot or shank.

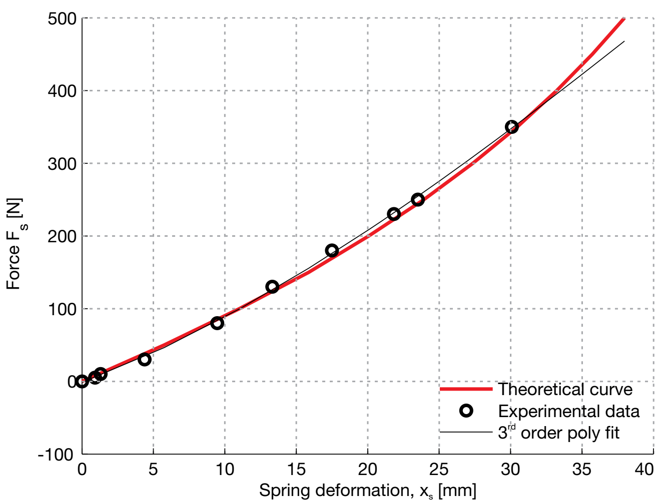

Figure 5: Graph of the force-travel of the lever-arm. The theoretical curve is obtained from the finite element model. The thin line is a 3rd order polynomial fit through experimentally obtained data points.

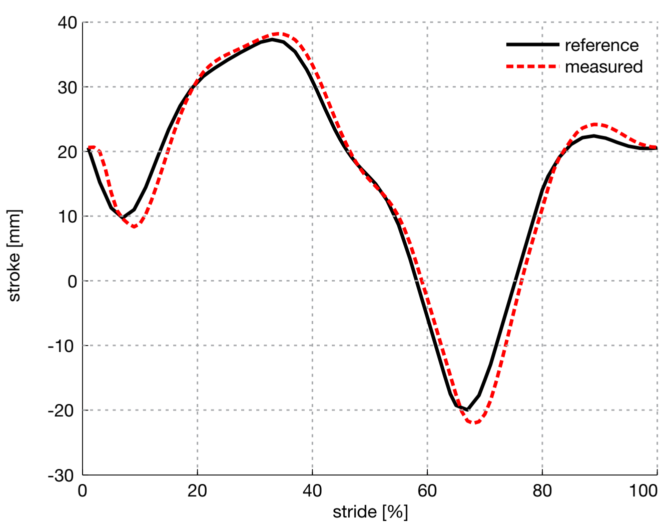

Figure 6: Experimental results of stroke tracking of the actuator. The reference trajectory is the optimized stroke trajectory.

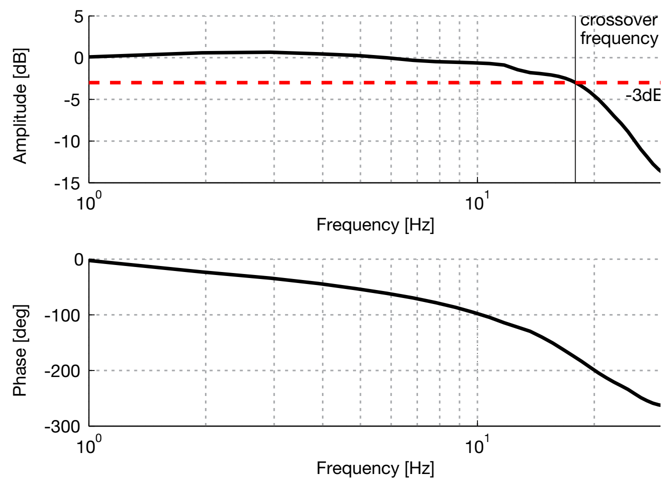

Figure 7: Bode magnitude and Bode phase plot from a sine sweep experiment with an amplitude of 1N. The bandwidth is determined by the point where the magnitude plot crosses the -3dB line.

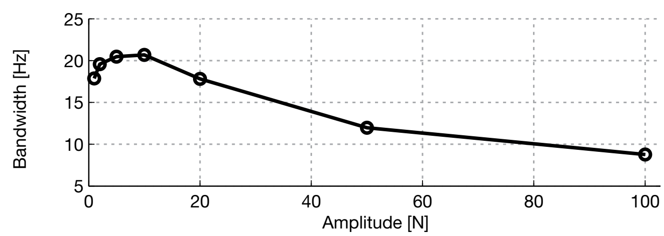

Figure 8: Experimentally determined force bandwidth of the actuator. at different force amplitudes.

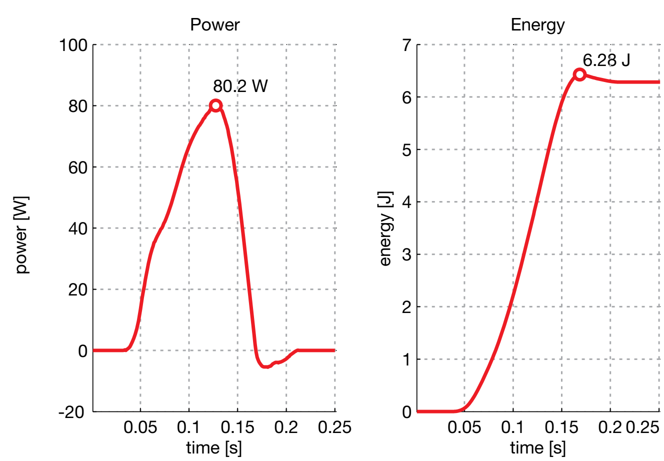

Figure 9 left: Experimental results of mechanical power delivered by the motor. right: The energy stored in the spring. The peak is caused by the release of kinetic energy when the motor inertia decelerates.

TABLE 4: COMPARISON OF DIFFERENT ANKLE EXOSKELETONS

Exoskeleton	Mass	Peak Power	Power Density	Autonomous
	[kg]	[W]	[W/kg]	
Kao et al. [19]	1.1	117[1]	115	no
Malcolm et al. [5]	0.7	95[2]	136	no
Norris et al. [6]	0.8	38.9[3]	48.6	no
Shorter et al.	1.9	25.9[4]	13.6	yes
Hitt et al. [12]	1.7	108[5]	63.5	yes
Achilles	***1.5***	***192[5]***	***128***	***yes***

For each exoskeleton the mass and the peak power are given. The power density is the ratio between the power and the mass of the exoskeleton. The rightmost column mentions if the exoskeleton is suitable for autonomous operation.

1 There are several slightly different versions of this exoskeleton.

2 Adapted from graphs in supplementary material of [5] where a normalized peak power of 1.35 W/kg is reported. This number is multiplied with a subject mass of 70 kg (mean plus standard deviation within the study).

3 The average peak power provided in an experimental study with young subjects.

4 Authors report 9.2 Nm peak torque supplied from 30 to 60 % of the gait cycle, multiplied with the maximum ankle speed of 2.81 rad/s from Winter data gives an indication of the power.

5 The theoretical mechanical power output.

The performance of the exoskeleton was assessed in multiple tests that simulated the operation conditions of the exoskeleton. The actual spring stiffness was very close to the spring stiffness in simulation. The actuator was able to track the designed stroke trajectory. Force tracking experiments revealed a bandwidth between 8.1 and 20.6 Hz. The maximal mechanical output power was 85.9% of the predicted maximal mechanical output (80.2W vs. 93.4W). If we assume a drop in performance with the same percentage, this indicates that the exoskeleton can provide 52.0% of the positive power at ankle push-off with a limited amount of added mass to the ankle. Based on the obtained results, we expect that the exoskeleton is suitable for its intended use: reducing the metabolic cost of walking with an autonomous exoskeleton. This will be evaluated on with human subjects in the near future.

REFERENCES

[1] D. Ferris, G. Sawicki, and M. Daley, "A physiologist's perspective on robotic exoskeletons for human locomotion," *Int. J. Humanoid Robot.*, vol. 4, no. 3, 2007.

[2] J. M. Donelan, R. Kram, and A. D. Kuo, "Mechanical work for step-to-step transitions is a major determinant of the metabolic cost of human walking," *J. Exp. Biol.*, vol. 205, no. 23, p. 3717, 2002.

[3] A. D. Kuo, J. M. Donelan, and A. Ruina, "Energetic consequences of walking like an inverted pendulum: step-to-step transitions.," *Exerc. Sport Sci. Rev.*, vol. 33, no. 2, pp. 88–97, Apr. 2005.

[4] G. S. Sawicki and D. P. Ferris, "Mechanics and energetics of level walking with powered ankle exoskeletons.," *J. Exp. Biol.*, vol. 211, no. Pt 9, pp. 1402–13, May 2008.

[5] P. Malcolm, W. Derave, S. Galle, and D. De Clercq, "A simple exoskeleton that assists plantarflexion can reduce the metabolic cost of human walking.," *PLoS One*, vol. 8, no. 2, p. e56137, Jan. 2013.

[6] J. A. Norris, K. P. Granata, M. R. Mitros, E. M. Byrne, and A. P. Marsh, "Effect of augmented plantarflexion power on preferred walking speed and economy in young and older adults," *Gait Posture*, vol. 25, no. 4, p. 620, 2007.

[7] Honda Motor Co. Ltd., "Honda Unveils Experimental Walking Assist Device With Bodyweight Support System," 2008. [Online]. Available: http://world.honda.com/news/2008/c081107Walking-Assist-Device/.

[8] Cyberdyne, "Robot Suit HAL," 2012. [Online]. Available: http://www.cyberdyne.jp/english/robotsuithal/index.html.

[9] R. C. Browning, J. R. Modica, R. Kram, and A. Goswami, "The effects of adding mass to the legs on the energetics and biomechanics of walking," *Med Sci Sport. Exerc.*, vol. 39, no. 3, pp. 515–25., 2007.

[10] J. H. Meuleman, E. H. van Asseldonk, and H. van der Kooij, "The effect of directional inertias added to pelvis and ankle on gait.," *J. Neuroeng. Rehabil.*, vol. 10, no. 1, p. 40, Apr. 2013.

[11] J. A. Blaya and H. Herr, "Adaptive control of a variable-impedance ankle-foot orthosis to assist drop-foot gait.," *IEEE Trans. Neural Syst. Rehabil. Eng.*, vol. 12, no. 1, pp. 24–31, Mar. 2004.

[12] J. Hitt, A. Oymagil, and T. Sugar, "Dynamically controlled ankle-foot orthosis (DCO) with regenerative kinetics: incrementally attaining user portability," in *IEEE International Conference on Robotics and Automation*, 2007, no. April, pp. 10–14.

[13] J. E. Pratt, B. T. Krupp, C. J. Morse, and S. H. Collins, "The RoboKnee: an exoskeleton for enhancing strength and endurance during walking," in *Robotics and Automation, 2004. Proceedings. ICRA '04. 2004 IEEE International Conference on*, 2004, vol. 3, pp. 2430–2435 Vol.3.

[14] K. W. Hollander, R. Ilg, T. G. Sugar, and D. Herring, "An efficient robotic tendon for gait assistance," *J. Biomech. Eng.*, vol. 128, no. 5, pp. 788–791.

[15] M. Ishikawa, P. V Komi, M. J. Grey, V. Lepola, and G.-P. Bruggemann, "Muscle-tendon interaction and elastic energy usage in human walking.," *J. Appl. Physiol.*, vol. 99, no. 2, pp. 603–8, Aug. 2005.

[16] S. Wang, C. Meijneke, and H. van der Kooij, "Modeling, design, and optimization of Mindwalker series elastic joint.," *IEEE Int. Conf. Rehabil. Robot.*, vol. 2013, pp. 1–8, Jun. 2013.

[17] D. A. Winter, *Biomechanics and motor control of human movement*, 2nd ed. Waterloo, Ontario, Canada: John Wiley and Sons, 1990, p. 52.

[18] H. Vallery, J. Veneman, R. Ekkelenkamp, M. Buss, and H. van der Kooij, "Compliant actuation of rehabilitation robots," *IEEE Robot. Autom. Mag.*, no. September, pp. 60–69, 2008.

[19] P.-C. Kao, C. L. Lewis, and D. P. Ferris, "Invariant ankle moment patterns when walking with and without a robotic ankle exoskeleton.," *J. Biomech.*, vol. 43, no. 2, pp. 203–9, Jan. 2010.